Inclusion Compounds of Cholic Acid with Aliphatic Esters

Mino R. Caira, Luigi R. Nassimbeni * and Janet L. Scott
Department of Chemistry, University of Cape Town, Rondebosch 7700, South Africa

The crystal structures and thermal analysis of cholic acid inclusion compounds with methyl acetate, ethyl acetate, ethyl propionate and *n*- and iso-propyl acetate are reported. Two packing modes occur and these are found to result in different differential scanning calorimetry traces which are explained by analysis of phase changes occurring on heating.

Cholic acid (3α,7α,12α-trihydroxy-5β-cholan-24-oic acid), CA, has recently attracted considerable attention as a host compound for a variety of guest molecules.

The structures of the monohydrate and the hemihydrate were characterised by Lessinger[1] and Lessinger and Low respectively,[2] while its inclusion compound with ethanol was described by Johnson and Schaefer.[3] The ability of cholic acid to form inclusion compounds with a wide range of guest molecules was announced by Miyata *et al.*,[4] and it was also shown that cholic acid can be used for the optical resolution of lactones.[5] We have previously reported the structures of cholic acid with methanol, ethanol and isopropyl alcohol and measured the enthalpies of the guest-release reactions[6] as well as the structures and selectivity study results with aniline and nitrobenzene.[7] We now present the results of the enclathration of cholic acid with selected aliphatic esters, and describe the structures and thermal stability of the inclusion compounds of cholic acid (CA), with methyl acetate (CAMA), ethyl acetate (CAET), *n*-propyl acetate (CAPAC), ethyl propionate (CAEP) and isopropyl acetate, (CAIP). Phase changes occurring during decomposition of some of the inclusion compounds are also reported and related to thermal events.

Experimental

Single crystals for X-ray diffraction measurements were grown by slow evaporation of solutions of CA dissolved directly in the liquid guest. In all cases the crystals selected were sealed in Lindemann capillary tubes together with the mother liquor to prevent desorption of the guest during data collection. Preliminary cell parameters were obtained photographically and intensity data were collected on an Enraf–Nonius CAD4 diffractometer at 294 K using graphite-monochromated Mo-Kα radiation, (λ = 0.7107 Å), and the $\omega - 2\theta$ scan mode. During each data collection three reference reflections were monitored periodically to check crystal stability. The data were corrected for Lorentz-polarisation effects. Refined unit cell parameters were obtained by least-squares analysis of 24 reflections measured on the diffractometer in the range $16 < \theta < 17°$. Crystal data and other experimental details are given in Table 1.

Structure Solution and Refinement.—All five structures were solved by direct methods using the program SHELX-86[8] and refined by full-matrix least-squares using the program SHELXL-93,[9] refining on F^2 (all data). *R*-factors based on observed structure factors larger than $4\sigma(F_o)$ as well as those based on F^2 of all data are presented in Table 1 for comparison with other structures. These are denoted R_1 and R_2 respectively or wR_1 and wR_2 for weighted *R*-factors. The weighting scheme used is shown as eqn. (1), where *a* and *b* are parameters defined

$$w = q/[\sigma^2(F_o^2) + (a \times P)^2 + b \times P] \quad (1)$$

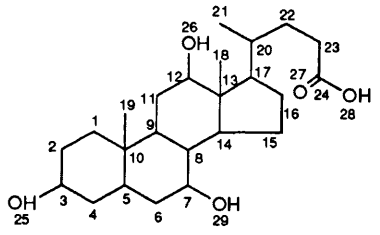

Cholic acid

for each structure and $P = [0.333\,33 \times \text{max. of } (0 \text{ or } F_o^2) + (1 - 0.333\,33) \times F_c^2]$. The weighting scheme was varied to minimise trends in the analysis of variance in terms of F_c^2.

Polar axis restraints after Flack and Schwarzenbach,[10] were employed to define the origin in these polar space groups. In the final model, most non-hydrogen atoms of the host were treated anisotropically although in cases where the atoms of the host carboxylic acid group exhibited unreasonably high anisotropic displacement parameters these atoms were refined isotropically. Disorder of the host carboxylic acid group is indicated in some cases although only O(27) of CAPAC was refined as disordered over two positions. In all cases the guest atoms were located unambiguously in a difference electron density map and refined with bond length and 'anti-bumping' restraints. Where necessary the atoms surrounding the sp^2 centre were restrained to planar geometry. Methine, methylene and methyl hydrogens of the host were subjected to restrained refinement with a common temperature factor for each type. Hydrogen atoms on the guest were only included if the guest was well refined. Particular care was taken with the location and refinement of the host hydroxy hydrogen atoms. In most cases, they were found in difference electron density maps but could not be refined satisfactorily without bond length and, in some cases, hydrogen-bonded distance restraints or at geometrically generated positions. In cases where the hydroxy hydrogen atoms could not be located in a difference electron density map they were omitted from the final model.

Tables of final fractional co-ordinates, H-atom positions and temperature factors, bond lengths, bond angles and structure factors have been deposited at the Cambridge Crystallographic Data Centre.†

Thermal Analysis.—Differential Scanning Calorimetry (DSC), and Thermal Gravimetry (TG), were performed on a Perkin-Elmer PC7 system. Crystals of the inclusion compounds

† For details of the deposition scheme, see 'Instructions for Authors (1994)', *J. Chem. Soc., Perkin Trans. 2*, Issue 1, 1994.

Table 1 Crystal and refinement data

	CAMA	CAET	CAEP	CAPAC	CAIP
Guest	Methyl acetate	Ethyl acetate	Ethyl propionate	*n*-Propyl acetate	Isopropyl acetate
H:G ratio	1:1	1:1	1:1	1:1	1:1
Molecular formula	$C_{27}H_{46}O_7$	$C_{28}H_{48}O_7$	$C_{29}H_{50}O_7$	$C_{29}H_{50}O_7$	$C_{29}H_{50}O_7$
M_r	482.66	496.69	510.71	510.71	510.71
Space group	$P\bar{1}$	$P2_1$	$P2_1$	$P2_1$	$P2_1$
Z	2	2	2	2	2
a/Å	12.223(2)	13.668(3)	13.571(1)	16.802(5)	16.604(3)
b/Å	8.189(1)	7.824(4)	7.969(1)	7.884(1)	7.979(3)
c/Å	14.204(2)	14.095(2)	14.237(1)	12.107(4)	12.141(2)
α/°	90.18(1)	90.0	90.0	90.0	90.0
β/°	105.72(2)	113.53(1)	113.53(1)	118.06(3)	117.76(2)
γ/°	94.03(1)	90.0	90.0	90.0	90.0
V/Å^3	1364(5)	1382(8)	1411(5)	1415(7)	1423(6)
D_c/g cm^{-3}	1.174	1.194	1.201	1.199	1.192
μ(Mo-Kα)/cm^{-1}	0.83	0.84	0.80	0.84	0.83
F(000)	528	544	560	560	560
Crystal dimensions/mm	0.3 × 0.4 × 0.4	0.2 × 0.3 × 0.5	0.3 × 0.3 × 0.4	0.5 × 0.5 × 0.5	0.4 × 0.3 × 0.3
Range					
h	−14 13	−16 14	−16 14	−13 19	−13 19
k	−9 9	0 9	0 9	0 9	−9 0
l	0 16	0 16	0 16	−13 14	−13 14
Std. reflections	3	3	3	3	3
Total exposure time/h	38.5	21.3	21.5	23.0	22.1
Intensity variation (%)	−8	−3.6	−6.4	−3.4	−6.9
No. of reflections collected	4885	2736	2699	2792	2810
No. of independent reflections	4879	2625	2705	2688	2705
No. of restraints	11	9	2	3	6
No. of parameters	584	284	283	340	318
Goodness of fit on F^2	1.050	1.036	1.034	1.027	1.029
R indices:					
$I > 2\sigma(I)$ R_1	0.0668	0.0732	0.0680	0.0700	0.0656
wR_2	0.1807	0.2042	0.1709	0.1880	0.1699
All data R_1	0.1265	0.1198	0.1175	0.1605	0.1306
wR_2	0.2195	0.2473	0.2044	0.2430	0.2061
Extinction coefficient	—	0.024(7)	—	—	—
$\Delta\rho_{max}$/e Å^{-3}	0.48	0.58	0.61	0.44	0.43
$\Delta\rho_{min}$/e Å^{-3}	−0.32	−0.39	−0.40	−0.35	−0.42

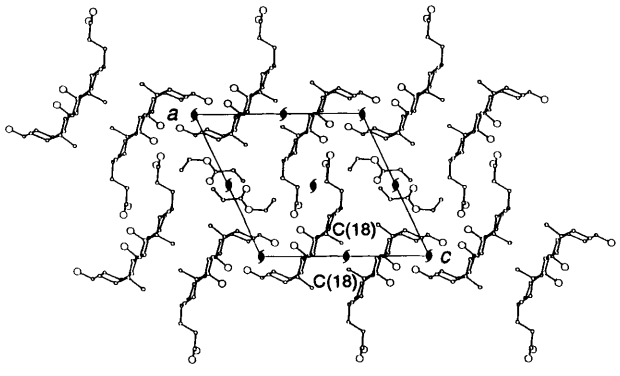

Fig. 1 Projection of CAEP along [010]

were removed from their mother liquor, blotted dry on filter paper and lightly crushed before analysis. Sample masses varied between 1 and 4 mg and were analysed over the temperature range 30 to 230 °C at a heating rate of 20 °C min^{-1}. The purge gas was dry nitrogen with a flow rate of 40 cm^3 min^{-1}.

X-Ray Powder Photography.—The X-ray diffraction (XRD) patterns of the inclusion compounds were recorded using a modified Weissenberg camera after Boeyens *et al.*[11] Decoupling movement of the sample from movement of the film allowed for continuous recording the XRD pattern while the temperature was slowly raised. Crushed samples were mounted in Lindemann capillary tubes with mother liquor. Tubes were not completely sealed to allow escape of the guest vapour and prevent pressure build-up. Samples were heated over the range 25–65 °C over a period of 3.5 h with constant monitoring of temperature and XRD patterns recorded with lateral film movement of 0.3 mm min^{-1}.

Results and Discussion

The five structures elucidated can be divided into two distinct groups, A and B. Group A comprises the structures CAMA, CAET and CAEP which have similar unit cell parameters, with CAMA slightly distorted from a monoclinic unit cell. The second group, B, comprises CAPAC and CAIP with unit cell parameters significantly different to group A. The differences between these two types are brought about by different stacking modes of the cholic acid bilayers. This is illustrated in Figs. 1 and 2, which display projections of CAEP and CAPAC along [010]. In CAEP the C(18) methyl groups stack in close proximity along the screw diad at 0, y, $\frac{1}{2}$, while in CAPAC the C(19) methyl groups are in close contact. This indicates a shift in the relative positions of the host bilayers and results in different orientations of the guest channels with respect to a in the respective unit cells. We have also noted that the guest molecules adopt different stacking modes in the two structure types. This is illustrated in Figs. 3 and 4 which depict the cross sections of the channels viewed approximately perpendicularly to the screw diads. In type A (*e.g.* CAEP), the guest molecules lie with their long molecular axis perpendicular to b, while in type B (*e.g.* CAPAC), the guest molecules adopt a herringbone pattern, with the long molecular axis approximately at 45° to b.

We have mapped the shapes of the channels by using the program OPEC.[12] The volume of the channel is analysed

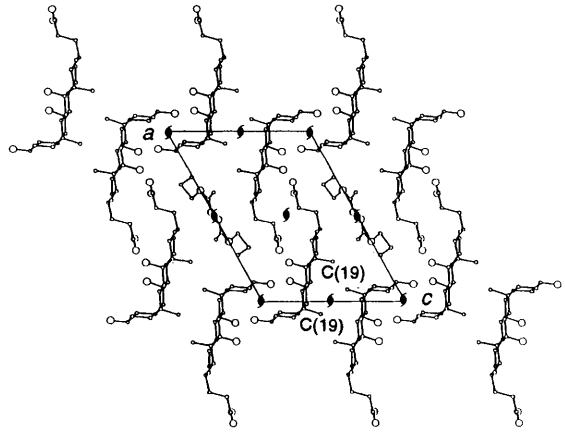

Fig. 2 Projection of CAPAC along [010]

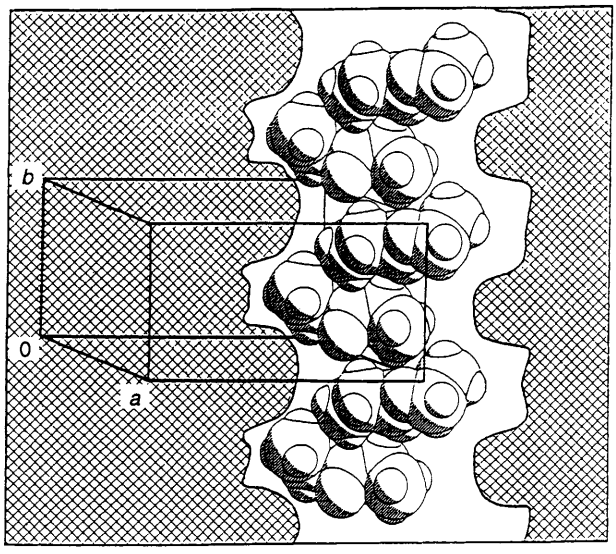

Fig. 3 Cross section of channel showing guest stacking mode, CAEP

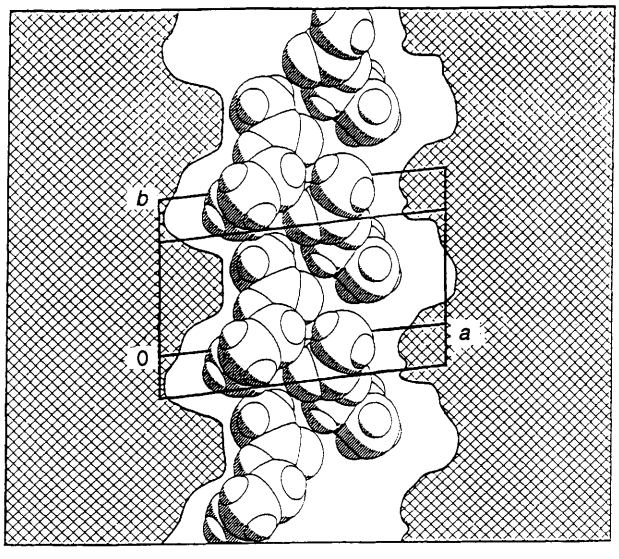

Fig. 4 Cross section of channel showing guest stacking mode, CAPAC

by applying a packing analysis routine in which all host atoms are assigned spherical volumes with radii equal to their van der Waals radii. The guest atoms are removed in the calculation and the channel is thus represented as unoccupied volume in the packing density maps.

The channels run parallel to the screw diads at $\frac{1}{2}$, y, 0 and are found to be more constricted between guests in type B

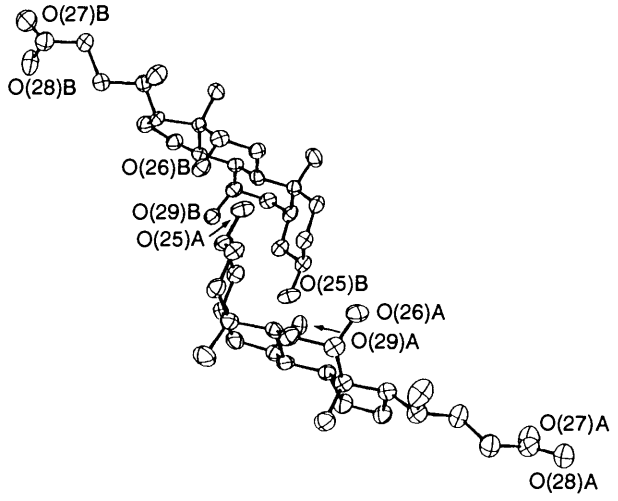

Fig. 5 Cholic acid host molecules in CAMA (50% enclosure ellipsoids)

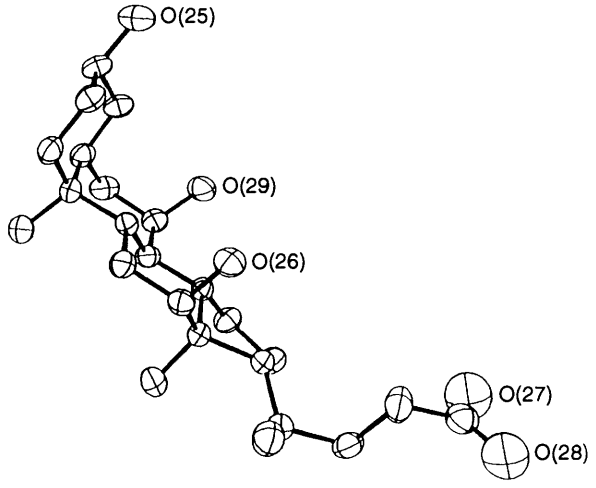

Fig. 6 Cholic acid host molecule in CAEP (50% enclosure ellipsoids)

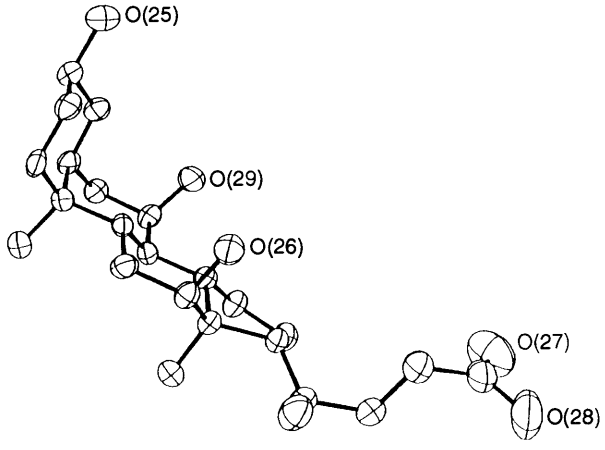

Fig. 7 Cholic acid host molecule in CAIP (50% enclosure ellipsoids)

structures. In CAMA, which crystallises in the space group $P1$, the channels are narrower better to accommodate the smaller guest molecules.

The bond lengths and angles of the cholic acid molecules are in good agreement with those found in previously determined structures. ORTEP plots of host molecules of the different structural types CAMA ($P1$, A-type), CAEP ($P2_1$, A-type) and CAIP ($P2_1$, B-type) with 50% enclosure ellipsoids are presented as Figs. 5 to 7. The configuration of the steroid nucleus is similar in each case but the flexible side chains adopt different positions.

Table 2 Torsion angles

	CAMA	CAET	CAEP	CAPAC	CAIP
τ_1 C(13)–C(17)–C(20)–C(21)	−52.6(9) −59.1(8)	−56.2(8)	−53.6(8)	−56.3(9)	−57.0(8)
τ_2 C(16)–C(17)–C(20)–C(22)	61.3(7) 60.4(7)	58.6(7)	57.1(7)	56.7(8)	56.5(7)
τ_3 C(13)–C(17)–C(20)–C(22)	−177.5(6) 179.2(5)	178.0(5)	179.1(5)	176.5(6)	176.7(5)
τ_4 C(17)–C(20)–C(22)–C(23)	−166.5(6) −159.4(6)	65.2(8)	65.7(7)	65.6(9)	62.9(8)
τ_5 C(21)–C(20)–C(22)–C(23)	67.2(9) 75.4(8)	−62.3(8)	−63.9(7)	−63.8(10)	−65.3(8)
τ_6 C(20)–C(22)–C(23)–C(24)	179.0(6) −174.7(6)	−168.7(7)	−172.5(6)	−169.0(8)	−174.7(9)
τ_7 C(22)–C(23)–C(24)–O(27)	−28.9(11) 132.6(8)	−107.0(10)	78.5(9)	−111.4(19)	86.3(10)
τ_8 C(22)–C(23)–C(24)–O(28)	150.5(6) −50.0(9)	71.7(9)	−100.9(8)	73.1(11)	−92.6(8)

Table 3 Hydrogen-bonding schemes

	CAMA					
	A–B	B–A	CAET	CAEP	CAPAC	CAIP
O(26) ··· O(27)	2.877(8)	2.855(6)		2.764(9)		2.779(8)
O(28) ··· O(26)			2.690(9)		2.711(9)	
O(25) ··· O(26)	2.768(6)	2.765(7)		2.837(7)		2.851(7)
O(26) ··· O(25)			2.800(6)		2.814(7)	
O(29) ··· O(25)	2.650(6)	2.687(6)		2.700(9)		2.685(7)
O(25) ··· O(29)			2.752(7)		2.726(9)	
O(28) ··· O(29)	2.648(7)	2.686(6)		2.748(6)		2.747(7)
O(29) ··· O(27)			2.800(9)		2.779(7)	

Table 4 Thermal analysis results

	CAMA	CAET	CAEP	CAPAC	CAIP
Guest	methyl acetate	ethyl acetate	ethyl propionate	*n*-propyl acetate	isopropyl acetate
TG weight loss observed (%)	15.53	17.31	19.16	19.19	19.67
TG weight loss calculated (%)	15.35	17.74	20.00	20.00	20.00
Normal boiling point of guest/°C	56.9	77	99	101.6	89
DSC endotherms/°C				47	45
			79	80[a]	92[a]
	114	104	113	112	114

[a] Diffuse peak.

We have analysed the torsion angles which determine the side chain configuration and these are listed in Table 2. While the majority of the torsion angles are remarkably constant, τ_4 and τ_5 in CAMA are significantly different, giving rise to the narrower channel accommodating the smaller guest. The torsion angle τ_7 [C(22)–C(23)–C(24)–O(27)], which describes the conformation of the carboxy group about the C(23)–C(24) bond is not consistent among the five structures, but varies in accordance with the requirements of the hydrogen bonding of the carboxy group. The two hydrogen bonding schemes are shown in Table 3. There is no barrier to free rotation about the C(23)–C(24) bond and two possible orientations of the carboxylic acid group, and consequently two possible H-bonding schemes, occur without causing significant differences in the overall structure. If O(28) and O(27) are interchanged this effect is transmitted throughout the H-bond network resulting in reversal of the donor and acceptor roles since O(27) (the carbonyl oxygen atom) must always act as an acceptor atom. The H-bond schemes are either: O(28)–H(28O) ··· O(26^{i}), O(26)–H(26O) ··· O(25^{ii}), O(25)–H(25O) ··· O(29^{ii}), O(29)–H29O) ··· O(27^{i}); (i) $-x-1, y-\frac{1}{2}, -z+1$, (ii) $-x+1, y+\frac{1}{2}, -z+2$, as in CAET or O(28)–H(28O) ··· O(29^{iii}),

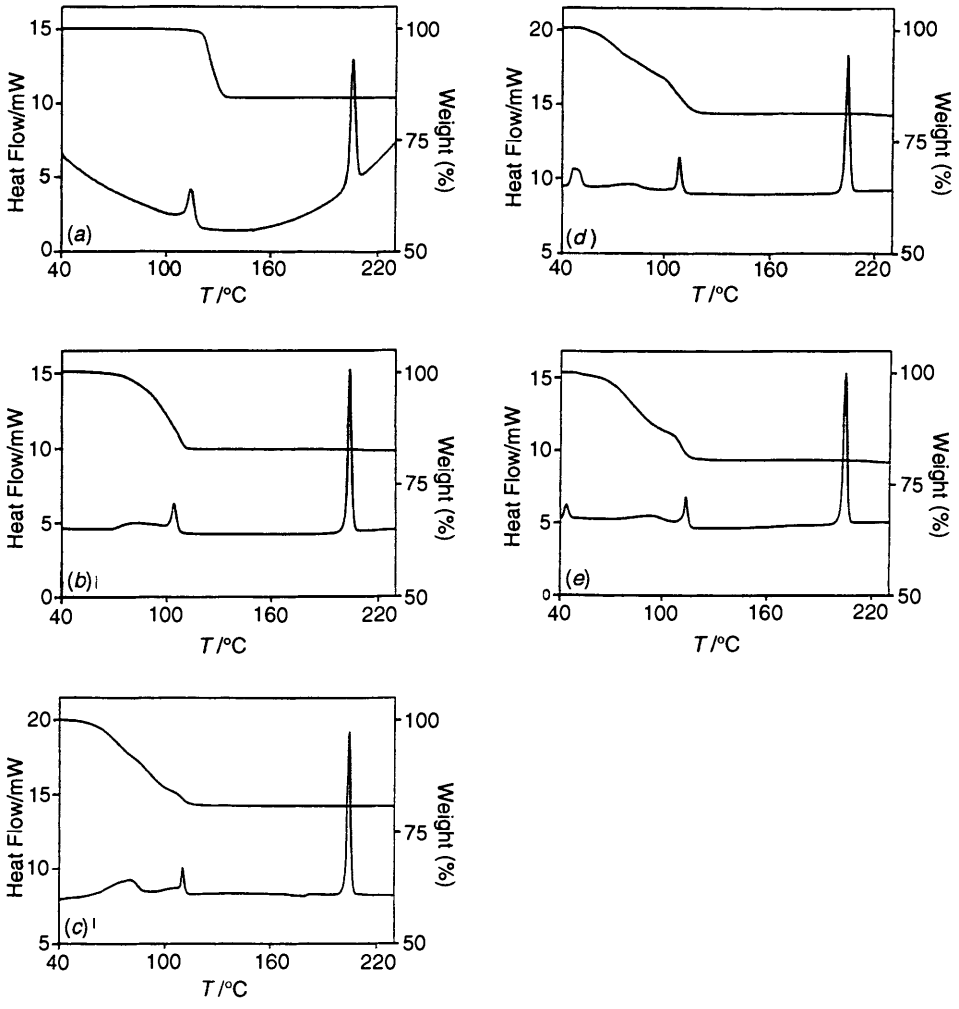

Fig. 8 TG and DSC traces of CA inclusion compounds with esters: (*a*) CAMA, (*b*) CAET, (*c*) CAEP, (*d*) CAPAC, (*e*) CAIP

O(29)–H(29O)···O(25^{iv}), O(25)–H(25O)···O(26^{v}), O(26)–H(26O)···O(27^{iii}); (iii) $-x-1, y+\frac{1}{2}, -z+1$, (iv) $-x, y+\frac{1}{2}, -z+2$, (v) $-x, y-\frac{1}{2}, -z+2$ as in CAIP. It is notable that CAEP appears to show disorder with respect to the H-bonding scheme associated with the disorder of the COOH group as evidenced by the averaged bond lengths obtained for C(24)–O(27) and C(24)–O(28). In this structure the hydroxy protons are not identified in difference maps. The different possibilities for H-bonding have no effect on the gross structure and either H-bonding scheme may occur in otherwise similar structures such as CAMA and CAET.

The thermal analysis results are shown in Table 4. There is good agreement between the calculated and observed weight losses for all five compounds, thus confirming their host:guest ratios as 1:1, as employed in the crystal structure refinement. The DSC traces of these compounds are complex indicating a number of endotherms. Many of the endotherms have leading tails rendering it difficult to determine onset temperatures and we therefore report the temperature of peak maxima in Table 4. The TG/DSC curves are shown in Fig. 8. CAMA exhibits an endotherm at 114 °C which may be ascribed to guest release and concomitant collapse to the CA(α) structure. In CAET this endotherm occurs at a slightly lower temperature and has a long leading tail beginning at approximately 70 °C. This may represent a well defined peak overlapping an earlier diffuse peak indicating the earlier onset of guest release as evidenced by the TG trace. Structures CAEP, CAPAC and CAIP all show endotherms with peaks at 112–113 °C and diffuse peaks in the region of 80–90 °C while CAIP and CAPAC show well defined

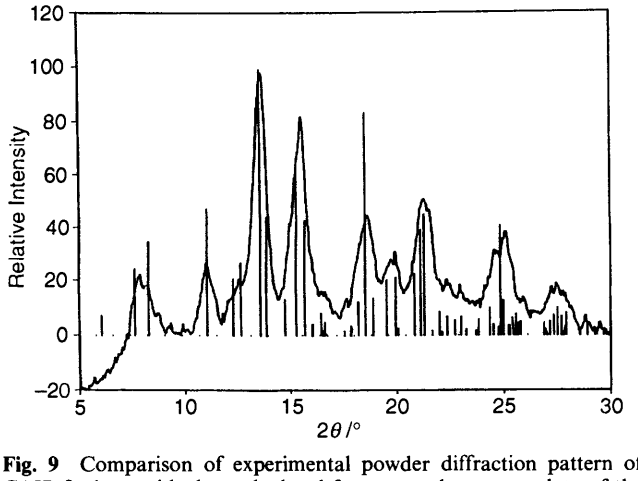

Fig. 9 Comparison of experimental powder diffraction pattern of CAIP β phase with that calculated from crystal structure data of the inclusion compound

endotherms at 45–47 °C. In an attempt to elucidate the structural changes occurring we considered changes in the powder X-ray diffraction patterns of these crystalline adducts. In all cases the experimental powder patterns of the host:guest complexes match well with those predicted from the crystal structures. A typical example of this is shown in Fig. 9. In the case of the A structures, the structure changes from that of the β phase directly to that of the α phase upon loss of guest. The B type structures, CAPAC and CAIP, however show an

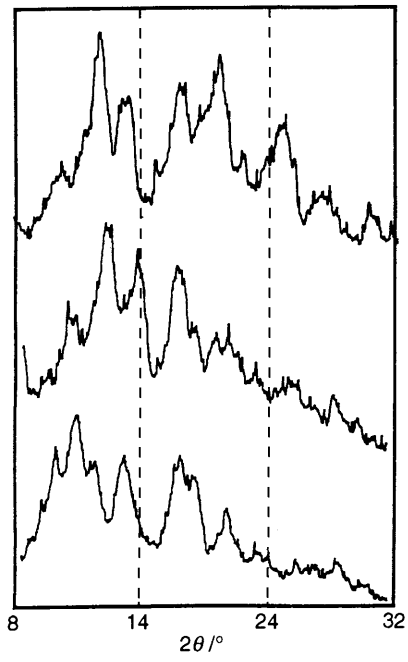

Fig. 10 Powder patterns of the three distinct phases, β, γ and α, exhibited by CAPAC

intermediate phase, designated γ, occurring after some guest is lost but at a temperature lower than that of the third DSC endotherm as shown in Fig. 10. This implies a sequence of events characterised by partial guest desorption resulting in a new phase followed by rearrangement to the CA(α) phase. All compounds revert to the α-phase upon complete guest desorption as the powder pattern of this phase is that of the host alone. All five structures show an endotherm corresponding to melting of the host at 201–204 °C.

We are carrying out further work on cholic acid inclusion compounds and related compounds such as those formed by the O(28) methyl ester of cholic acid. This host has the ability to entrap acetonitrile from the vapour phase much faster than the parent cholic acid. We are thus measuring the kinetics of enclathration in order to relate these to the structures.

References

1 L. Lessinger, *Cryst. Struct. Commun.*, 1982, **11**, 1787.
2 L. Lessinger and B. W. Low, *J. Crystallogr. Spectrosc. Res.*, 1993, **23**, 85.
3 Paul L. Johnson and John P. Schaefer, *Acta Crystallogr., Sect. B*, 1972, **28**, 3083.
4 M. Miyata, M. Shibakami, W. Goonewardena and K. Takemoto, *Chem. Lett.*, 1987, 605.
5 M. Miyata, M. Shibakami and K. Takemoto, *J. Chem. Soc., Chem. Commun.*, 1988, 655.
6 E. Jones and L. R. Nassimbeni, *Acta Crystallogr., Sect. B*, 1990, **46**, 399.
7 M. R. Caira, L. R. Nassimbeni and J. L. Scott, *J. Chem. Soc., Chem. Commun.*, 1993, 612.
8 G. M. Sheldrick, SHELX-86, *Crystallographic Computing 3*, eds. G. M. Sheldrick, C. Kruger and R. Goddard, Oxford University Press, 1985, p. 175.
9 G. M. Sheldrick, SHELXL-93: *A Program for Crystal Structure Determination, J. Appl. Crystallogr.*, in preparation, 1993.
10 H. D. Flack and D. Schwarzenbach, *Acta Crystallogr., Sect. A*, 1988, **44**, 499.
11 Jan C. A. Boeyens, Ernst Ferg, Demetrius C. Levendis and F. R. Ludwig Schöning, *S. Afr. J. Chem.*, 1991, **44**, 42.
12 A. Gavezzotti, *J. Am. Chem. Soc.*, 1983, **105**, 5220.

Paper 3/03819J
Received 2nd *July* 1993
Accepted 22nd *November* 1993